Internal Josephson effects in spinor dipolar Bose-Einstein condensates

Masashi Yasunaga and Makoto Tsubota*
Department of Physics, Osaka City University, Sumiyoshi-ku, Osaka 558-8585, Japan
(Received 9 December 2009; published 24 February 2010)

We theoretically study the internal Josephson effect, which is driven by spin-exchange interactions and magnetic dipole-dipole interactions, in a three-level system for spin-1 Bose–Einstein condensates, obtaining novel spin dynamics. We introduce single spatial mode approximations into the Gross–Pitaevskii equations and derive the Josephson-type equations, which are analogous to tunneling currents through three junctions between three superconductors. From an analogy with two interacting nonrigid pendulums, we identify unique varied oscillational modes, called the 0–π, 0–*running*, *running*–*running*, $2n\pi$ & *running*–2π, *single nonrigid pendulum*, and *two rigid pendulums* phase modes. These Josephson modes in the three states are expected to be found in real atomic Bose gas systems.

DOI: 10.1103/PhysRevA.81.023624 PACS number(s): 03.75.Mn, 03.75.Kk

I. INTRODUCTION

The Josephson effect is a universal quantum phenomenon, defined as a current between two or more macroscopic quantum states with weak coupling driven by the relative phases of the macroscopic wave functions. The effect for a junction of two superconductors was originally predicted by Josephson [1] and discovered by Anderson and Rowell [2]. When the effect was first predicted and discovered, it was considered a characteristic phenomenon of superconductors. However, the effect has been found in diverse fields since Feynman redefined the Josephson effect as the quantum tunneling between two levels [3]. In particular, Maki and Tsuneto have considered nonlinear ringing between equal spin pairing states $|\uparrow\uparrow\rangle$ and $|\downarrow\downarrow\rangle$ in superfluid ^{3}He-A as a Josephson junction between the internal degrees of freedom [4]. Webb *et al.* subsequently observed the effect by NMR [5].

Such Josephson effects have also been studied in atomic Bose–Einstein condensates (BECs). Smerzi *et al.* derived Josephson-type equations in a double-well potential from Gross–Pitaevskii (GP) equations with two-mode approximations, revealing three oscillations, namely the 0, π, and *running* phase modes [6,7]. Macroscopic quantum self-trapping from the *running* mode and ac Josephson effects from the 0 phase mode have been observed by Albiez *et al.* [8]. Furthermore, Zhang *et al.* considered transitions between three energy states for spin-1 BECs driven by spin-exchange interactions as internal Josephson effects [9] and Chang *et al.* observed the internal Josephson oscillation [10].

In addition, studies have focused on the magnetic dipole–dipole interaction (MDDI) in BECs. The interaction between spins has a characteristic symmetry for spin and orbit. Therefore, the interaction is theoretically expected to give new quantum phases [11–13], the Einstein–de Haas effect [14], and so on. Griesmaier *et al.* realized spinor dipolar condensates using ^{52}Cr atoms [15], which have larger magnetic moments than alkali atoms. The condensates clearly show shape-dependent anisotropy of the MDDI [16,17]. Thus, the study of the MDDI has opened new avenues for investigating spinor condensates.

For the MDDI, we can demonstrate new internal Josephson effects in spin-1 BECs. The internal Josephson effect without the MDDI is analogous with two junctions between three superconductors because the weak coupling, namely the spin-exchange interaction, permits transitions only from $|0\rangle$ to $|\pm1\rangle$ and from $|\pm1\rangle$ to $|0\rangle$. However, it is possible to transfer from $|\pm1\rangle$ to $|\mp1\rangle$ if the MDDI drives the transitions because the anisotropic interaction breaks the conservation law of magnetization, as will be discussed later. As the previous study, Cheng *et al.* have discussed the Josephson effects driven by the MDDI in the conservation law [18]. Therefore, we consider out of the law that the transitions through the MDDI are analogous with Josephson effects for three circular junctions between three superconductors (see Fig. 1).

In this article, we introduce the spin dynamics in spinor dipolar BECs in Sec. II using the GP equations with single-mode approximations, and we demonstrate new Josephson oscillations in Sec. III. Section IV is devoted to a conclusion.

II. FORMULATION

A. Single-mode approximation

Before we consider the internal Josephson effect for spin-1 BECs, we analyze the spin-1 GP equations with an MDDI:

$$\begin{aligned} i\hbar\frac{\partial\psi_\alpha}{\partial t} &= \left(-\frac{\hbar^2}{2M}\nabla^2 + V - \mu\right)\psi_\alpha - g_e\mu_B\mathbf{H}\cdot\mathbf{F}_{\alpha\beta}\psi_\beta \\ &\quad + c_0\psi^*_\beta\psi_\beta\psi_\alpha + c_2\mathbf{F}\cdot\mathbf{F}_{\alpha\beta}\psi_\beta \\ &\quad + c_{dd}\int d\mathbf{r}'\frac{\delta_{ij} - 3e^ie^j}{|\mathbf{r}-\mathbf{r}'|^3}F_i(\mathbf{r}')F^j_{\alpha\beta}\psi_\beta, \end{aligned} \tag{1}$$

where the integers α and β represent the spin 0 and ±1 states, $V(\mathbf{r})$ is the trapping potential, and μ is the chemical potential. The spin-density vector $\mathbf{F} = (F_x, F_y, F_z)$ and the vector of the spin components $\mathbf{F}_{\alpha\beta} = (F^x_{\alpha\beta}, F^y_{\alpha\beta}, F^z_{\alpha\beta})$ are represented by $F_{i=x,y,z} = \psi^*_\alpha F^i_{\alpha\beta}\psi_\beta$ given by the components $F^i_{\alpha\beta}$ of the spin matrices $\hat{F}_i$ for spin-1. The Zeeman term is presented by Lande's g factor of an electron g_e, Bohr magneton μ_B, and external magnetic field $\mathbf{H}$. The coefficients $c_0 = (g_0 + 2g_2)/3$

*tsubota@sci.osaka-cu.ac.jp

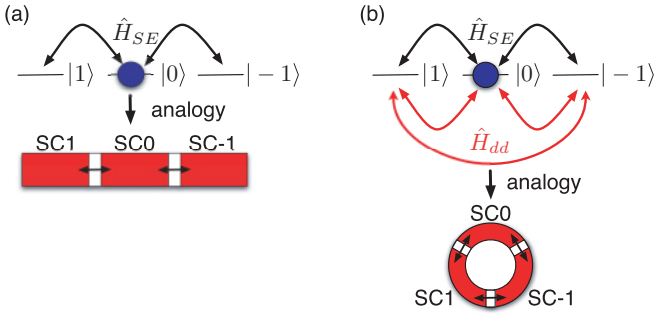

FIG. 1. (Color online) The transitions, driven by the Hamiltonians of a spin-exchange interaction $\hat{H}_{SE}$ (black arrows) and an MDDI $\hat{H}_{dd}$ [red (dark gray) arrows], between the energy states (solid line) are analogous to the Josephson effect for cooper pairs tunneling through (a) two and (b) three insulators (white boxes) between superconductors, named SC1, SC0, and SC-1 [red (dark gray) boxes]. (a) and (b) compare differently with the MDDI, whereas the MDDI can also drive transition from $|\pm1\rangle$ to $|\mp1\rangle$. The circles represent the condensate.

and $c_2 = (g_2 - g_0)/3$ are the interaction parameters for $g_i = 4\pi\hbar^2 a_i/M$ represented by the s-wave scattering lengths a_i. The coefficient of the MDDI is given by $c_{dd} = \mu_0 g_e^2 \mu_B^2/4\pi$ with $\mathbf{e} = (\mathbf{r} - \mathbf{r}')/|\mathbf{r} - \mathbf{r}'|$ being a unit vector.

Since it is difficult to derive the internal Josephson effect from Eq. (1) directly, we introduce the single-mode approximation [9]:

$$\psi_i(\mathbf{r}, t) = \sqrt{N}\xi_i(t)\phi(\mathbf{r}) \exp\left(-\frac{i\mu t}{\hbar}\right), \tag{2}$$

where ϕ satisfies the eigenvalue equation $(-\hbar^2\nabla^2/2M + V + c_0 n)\phi = \mu\phi$ with the relation $\int d\mathbf{r}|\phi|^2 = 1$. The approximation can be used when the shapes of the condensates are decided by the spin-independent terms, namely $|c_0| \gg |c_2|$. The condition is satisfied for ^{87}Rb and ^{23}Na. The validity of the approximation in spin-1 dipolar BECs has been discussed by Yi and Pu [19]. They found that the approximation is affected by the anisotropic parameter of the shape of the condensates λ and the ratio $c_{dd}/|c_2|$. For small λ, the approximation is well defined even if the ratio is large. Here, we assume that the ratio is smaller than 1, allowing the approximation to be used. Hence, introducing Eq. (2) into Eq. (1), we can derive the equation of the spinor $|\xi\rangle = (\xi_1, \xi_0, \xi_{-1})^T$ in $\mathbf{H} = H\hat{z}$,

$$i\hbar\frac{d}{dt}|\xi\rangle = (\hat{H}_Z + \hat{H}_{SE} + \hat{H}_{dd})|\xi\rangle, \tag{3}$$

given by the Zeeman, the spin-exchange interaction, and the MDDI Hamiltonians,

$$\hat{H}_Z = -g_e\mu_B \begin{pmatrix} H & 0 & 0 \\ 0 & 0 & 0 \\ 0 & 0 & -H \end{pmatrix}, \tag{4}$$

$$\hat{H}_{SE} = c \begin{pmatrix} 1-2\rho_{-1} & \rho_{-10} & 0 \\ \rho_{0-1} & 1-\rho_0 & \rho_{01} \\ 0 & \rho_{10} & 1-2\rho_1 \end{pmatrix}, \tag{5}$$

$$\hat{H}_{dd} = c_{dd}^{+} \begin{pmatrix} \rho_0 & \rho_{-10} & 0 \\ \rho_{0-1} & 1-\rho_0 & \rho_{01} \\ 0 & \rho_{10} & \rho_0 \end{pmatrix} + c_{dd}^{-} \begin{pmatrix} 0 & \rho_{10} & \rho_0 \\ \rho_{01} & \rho_{-11}+\rho_{1-1} & \rho_{0-1} \\ \rho_0 & \rho_{-10} & 0 \end{pmatrix} + 2c_{dd}^{z} \begin{pmatrix} m & 0 & 0 \\ 0 & 0 & 0 \\ 0 & 0 & -m \end{pmatrix}, \tag{6}$$

where $\rho_{ij} = \xi_i^*\xi_j$ ($\rho_{ii} = \rho_i$) are components of the density matrix $\rho = |\xi\rangle\langle\xi|$, $c_{dd}^{\pm} = c_{dd}^{x} \pm c_{dd}^{y}$ with c_{dd}^{z} given by

$$c_{dd}^{i} = \frac{c_{dd}}{2} N \iint d\mathbf{r}d\mathbf{r}' \frac{|\phi(\mathbf{r})|^2|\phi(\mathbf{r}')|^2}{|\mathbf{r}-\mathbf{r}'|^3}\left(1 - 3e^i \sum_j e^j\right), \tag{7}$$

$c = c_2 N \int d\mathbf{r}|\phi|^4$ are the interaction parameters, and $m = \rho_1 - \rho_{-1}$ is the magnetization. Comparing Eq. (5) with Eq. (6), we can conclude that the term with c_{dd}^{-} in $\hat{H}_{dd}$ includes the operators $|\pm1\rangle\langle\mp1|$, which project from $|\mp1\rangle$ to $|\pm1\rangle$, where $|1\rangle = (1,0,0)^T$, $|-1\rangle = (0,0,1)^T$ are unit vectors. These operators are not included in $\hat{H}_{SE}$. We again emphasize that the transition from $|\pm1\rangle$ to $|\mp1\rangle$ is possible only by the MDDI.

Using the relation $\sum_i \rho_i = 1$, we can rewrite the spin exchange and the dipole term to give

$$\hat{H}_{SE} + \hat{H}_{dd} = (c + c_{dd}^{+}) \begin{pmatrix} \rho_0 & \rho_{-10} & 0 \\ \rho_{0-1} & 1-\rho_0 & \rho_{01} \\ 0 & \rho_{10} & \rho_0 \end{pmatrix} + c_{dd}^{-} \begin{pmatrix} 0 & \rho_{10} & \rho_0 \\ \rho_{01} & \rho_{-11}+\rho_{1-1} & \rho_{0-1} \\ \rho_0 & \rho_{-10} & 0 \end{pmatrix} + (c + 2c_{dd}^{z}) \begin{pmatrix} m & 0 & 0 \\ 0 & 0 & 0 \\ 0 & 0 & -m \end{pmatrix}. \tag{8}$$

Equation (8) clearly shows that a c term can be included in the c_{dd}^{+} and c_{dd}^{z} terms. In short, the MDDI is partly renormalized in the spin-exchange interaction.

In conclusion for the MDDI, three important roles for spin dynamics appear in Eq. (6). The first is the spin-exchange effect, as in Eq. (5), given by the c_{dd}^{+} and c_{dd}^{z} terms of $\hat{H}_{dd}$. The second is the transition from the ±1 to the ∓1 states, given by the c_{dd}^{-} term. The last is an interaction between the magnetization and the spin, given by the c_{dd}^{z} term, which implies that the magnetization produces a molecular field.

B. Josephson-type equations

In order to investigate the Josephson effect for transitions between the three states, we substitute $\xi_j = \sqrt{\rho_j}e^{i\theta_j}$ in Eq. (3), deriving the Josephson-type equations for ρ_0, m and relative

phases $\theta = \theta_1 + \theta_{-1} - 2\theta_0$ and $\theta_m = \theta_1 - \theta_{-1}$;

$$\dot{\rho_0} = \frac{2}{\hbar} c' \rho_0 \sqrt{(1-\rho_0)^2 - m^2} \sin\theta + \frac{2}{\hbar} c_{dd}^- \rho_0 \{(1-\rho_0)\sin\theta\cos\theta_m + m\cos\theta\sin\theta_m\}, \quad (9)$$

$$\dot{m} = -\frac{2}{\hbar} c_{dd}^- \rho_0 \{\sqrt{(1-\rho_0)^2 - m^2}\sin\theta_m + (1-\rho_0)\cos\theta\sin\theta_m + m\sin\theta\cos\theta_m\}, \quad (10)$$

$$\dot{\theta} = \frac{2}{\hbar} c'(1-2\rho_0) + \frac{2}{\hbar} c' \frac{(1-\rho_0)(1-2\rho_0) - m^2}{\sqrt{(1-\rho_0)^2 - m^2}} \cos\theta + \frac{2}{\hbar} c_{dd}^- \left\{ \frac{(1-\rho_0)(1-2\rho_0) - m^2}{\sqrt{(1-\rho_0)^2 - m^2}} \cos\theta_m + (1-2\rho_0)\cos\theta\cos\theta_m - m\sin\theta\sin\theta_m \right\}, \quad (11)$$

$$\dot{\theta_m} = -\frac{2}{\hbar}(E_Z + c''m) + \frac{2}{\hbar} c' \frac{m\rho_0}{\sqrt{(1-\rho_0)^2 - m^2}} \cos\theta + \frac{2}{\hbar} c_{dd}^- \left\{ \frac{m\rho_0}{\sqrt{(1-\rho_0)^2 - m^2}} \cos\theta_m + \rho_0 \sin\theta \sin\theta_m \right\}, \quad (12)$$

where $E_Z = -g_e \mu_B H$ is the Zeeman energy and $c' = c + c_{dd}^+$ and $c'' = c + 2c_{dd}^z$ are the interaction coefficients. The equations clearly demonstrate the definition of the Josephson effect, namely a current between states driven by a relative phase.

First, from Eq. (10), we can easily see that conservation of the magnetization is broken by the c_{dd}^- term. When $c_{dd}^- = 0$, the magnetization becomes a conserved value. Under the single-mode approximation, $c_{dd}^i = 0$ for uniform density and a spherical shape, which is obtained from the integration, Eq. (7). Second, we note that the variables ρ_0 and m are canonical conjugates of θ and θ_m, respectively. Therefore, these equations can be derived from the canonical equations of motions:

$$\dot{\rho_0} = -\frac{2}{\hbar}\frac{\partial \mathcal{H}}{\partial \theta}, \quad \dot{\theta} = \frac{2}{\hbar}\frac{\partial \mathcal{H}}{\partial \rho_0}, \quad \dot{m} = \frac{2}{\hbar}\frac{\partial \mathcal{H}}{\partial \theta_m}, \quad \text{and} \quad \dot{\theta_m} = -\frac{2}{\hbar}\frac{\partial \mathcal{H}}{\partial m},$$

whose Hamiltonian is represented as

$$\mathcal{H} = \mathcal{H}_\theta + \mathcal{H}_{\theta_m} + \mathcal{H}_{\rm int}, \quad (13)$$

where

$$\mathcal{H}_\theta = c'\{\rho_0(1-\rho_0) + \rho_0\sqrt{(1-\rho_0)^2 - m^2}\cos\theta\}, \quad (14)$$

$$\mathcal{H}_{\theta_m} = \frac{c''}{2}m^2 + E_z m + c_{dd}^- \rho_0 \sqrt{(1-\rho_0)^2 - m^2}\cos\theta_m, \quad (15)$$

$$\mathcal{H}_{\rm int} = c_{dd}^-\{\rho_0(1-\rho_0)\cos\theta\cos\theta_m - \rho_0 m\sin\theta\sin\theta_m\}. \quad (16)$$

Since the Hamiltonian $\mathcal{H}(\rho_0(t), m(t), \theta(t), \theta_m(t))$ is not explicitly time dependent, the relation $d\mathcal{H}/dt = \partial\mathcal{H}/\partial t = 0$ is satisfied. A comparison of the Hamiltonian with that of a pendulum of length l and angle φ, $\mathcal{H}_p(P,\varphi) = P^2/2M + Mgl\cos\varphi$, shows that the dynamics described by the equations may be equal to that of two nonrigid pendulums, because $\mathcal{H}_\theta$ and $\mathcal{H}_{\theta_m}$ are similar to the Hamiltonian of nonrigid pendulums with lengths proportional to $c'\rho_0\sqrt{(1-\rho_0)^2 - m^2}$ and $c_{dd}^-\rho_0\sqrt{(1-\rho_0)^2 - m^2}$ and angles θ and θ_m, respectively. The two pendulums have some interaction with each other, represented by terms in $\mathcal{H}_{\rm int}$ that include the product of θ by θ_m. Therefore, we consider that Eq. (13) represents the Hamiltonian of two interacting nonrigid pendulums (see Fig. 2).

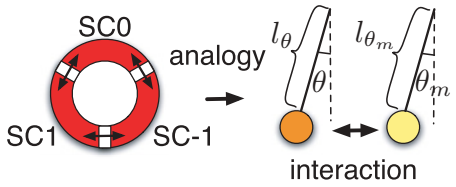

FIG. 2. (Color online) Analogy between the dynamics of Josephson junctions and two interacting nonrigid pendulums with lengths $l_\theta \propto c'\rho_0\sqrt{(1-\rho_0)^2 - m^2}$ and $l_{\theta_m} \propto (c_{dd}^-/c')l_\theta$.

III. SPIN DYNAMICS

In this section, we discuss solutions of the equations for $E_Z = 0$, namely small oscillations of two nonrigid pendulums in Sec. III A, oscillations of a single nonrigid pendulum in Sec. III B, and oscillations of two interacting nonrigid pendulums in Sec. III C.

A. Small oscillation around stationary solutions

Not being able to solve the Josephson-type equation directly, we first obtain the solutions for the stationary states:

$$\rho_0 = \rho_a, \quad m = 0, \quad \theta = (2n+1)\pi, \quad \theta_m = \theta_a \quad (17)$$

and

$$\rho_0 = \tfrac{1}{2}, \quad m = 0, \quad \theta = 2n\pi, \quad \theta_m = n\pi. \quad (18)$$

Here ρ_a and θ_a are arbitrary constants. For $E_Z = 0$, we cannot obtain the stationary magnetization $m \neq 0$. In order to study the features of the oscillation of the pendulums, we perform linear analysis by introducing the approximations $\rho_0 \simeq \rho_{0s} + \delta\rho_0$, $m \simeq m_s + \delta m$, $\theta \simeq \theta_s + \delta\theta$, and $\theta_m \simeq \theta_{ms} + \delta\theta_m$, where these deviations from the stationary solutions are very small, into the Josephson-type equations. Linearizing the equations by ignoring squares of the deviations, we obtain the equations for the deviations; the solutions around Eq. (17) are

$$\delta\dot{m} = \delta\dot{\theta} = 0, \quad (19)$$

and those around Eq. (18) are

$$\delta\ddot{\rho}_0 = -\omega_{\rho_0\pm}^2 \delta\rho_0, \quad (20)$$

$$\delta\ddot{m} = -\omega_{m\pm}^2 \delta m \quad (21)$$

where $\omega_{\rho_0\pm}^2 = 4(c' \pm c_{dd}^-)^2/\hbar^2$ and $\omega_{m\pm}^2 = 4c_{dd}^-\{\mp c_{dd}^z \pm (c_{dd}^+ \pm c_{dd}^-)/2\}/\hbar^2$ with $\pm$ indicating the equations for $\theta_{ms} = 2n\pi$ and $(2n+1)\pi$, respectively. From Eq. (19), we can conclude that there are no stable oscillational solutions around Eq. (17). On the other hand, Eqs. (20) and (21) are easily solved and have the solutions $\delta\rho_0 = \Delta_\rho \cos\omega_{\rho\pm}t$ and $\delta m =$

$\Delta_m \cos \omega_{m\pm} t$, whose amplitudes are Δ_ρ and Δ_m. Considering the deviations from Eqs. (19) to (21), we can conclude that there are no oscillations around $\theta = (2n+1)\pi$, namely the π phase mode in the canonically conjugate variable $\{\rho_0, \theta\}$, whereas there are 0 and π phase modes in $\{m, \theta_m\}$.

B. Josephson effect for a nonrigid pendulum

Next, in order to review the 0, π, and *running* phase modes in spin-1 BECs, we study the Josephson effect for $c_{dd}^- = 0$ obtained for spherically shaped condensates [20]. Under this condition, the spin dynamics are represented by Eqs. (9) and (10) with $c_{dd}^- = 0$, where there is no need to consider $\dot{m}$ and $\dot{\theta_m}$ because m is constant. The equations are the same as for the Josephson effect driven by the spin-exchange interaction in Ref. [9] if the quadratic Zeeman effect, which is effective for the hyperfine interaction between the nuclear and electron spins in the Zeeman splits [10,21], is introduced in the equation. Therefore, considering the quadratic Zeeman effect $\delta_{dd} \propto H_{eff}^2$ given by the effective dipole magnetic field $H_{eff} \propto c_{dd}^z m$, we obtain

$$\dot{\rho}_0 = \frac{2}{\hbar} c' \rho_0 \sqrt{(1-\rho_0)^2 - m^2} \sin\theta, \tag{22}$$

$$\dot{\theta} = -\frac{2}{\hbar}\delta_{dd} + \frac{2}{\hbar}c'(1-2\rho_0) + \frac{2}{\hbar}c' \frac{(1-\rho_0)(1-2\rho_0) - m^2}{\sqrt{(1-\rho_0)^2 - m^2}} \cos\theta, \tag{23}$$

where ρ_0 is the canonical conjugate of θ. Hence, these equations are derived from the canonical equations of motions for the Hamiltonian:

$$\mathcal{H}' = \delta_{dd}(1-\rho_0) + c'\{\rho_0(1-\rho_0) + \rho_0\sqrt{(1-\rho_0)^2 - m^2}\cos\theta. \tag{24}$$

The Hamiltonian directly represents the system of a nonrigid pendulum. Using $\mathcal{H}' = \mathcal{H}'_0 = \mathcal{H}'[\rho_0(0), \theta(0)]$ for $\dot{\mathcal{H}}' = 0$, we can solve Eq. (22) and obtain the solutions expressed by Jacobi's elliptic function $\mathrm{cn}(a, k)$; for $c' > 0$

$$\rho_0 = \rho_b + (\rho_c - \rho_b)\mathrm{cn}^2\left(\frac{1}{\hbar}\sqrt{2c'\delta_{dd}(\rho_c - \rho_a)}t, k\right), \tag{25}$$

and for $c' < 0$

$$\rho_0 = \rho_b - (\rho_b - \rho_a)\mathrm{cn}^2\left(\frac{1}{\hbar}\sqrt{-2c'\delta_{dd}(\rho_c - \rho_a)}t, k'\right), \tag{26}$$

where $k = \{(\rho_c - \rho_b)(\rho_c - \rho_a)\}^{1/2}$ and $k' = \{(\rho_b - \rho_a)/(\rho_c - \rho_a)\}^{1/2}$ are given by the roots of $\dot{\rho}_0 = 0$, $\rho_{a,b,c}$. Pendulumlike oscillations occur on the contour lines of Eq. (24) for energy being conserved, shown in Fig. 3. The dynamics can be classified into three modes; the dynamics on the lines around $\theta = 0$ and π are called the 0 and π phase modes, respectively, and the line from $\theta = -2\pi$ to 2π is the *running* phase mode. The 0 phase mode corresponds to the motion of a pendulum oscillating around $\theta = 0$ with a varying length. The π phase mode also shows an oscillation around $\theta = \pi$, a characteristic dynamics for the nonrigid pendulum. Finally, the *running* phase mode represents the rotational dynamics.

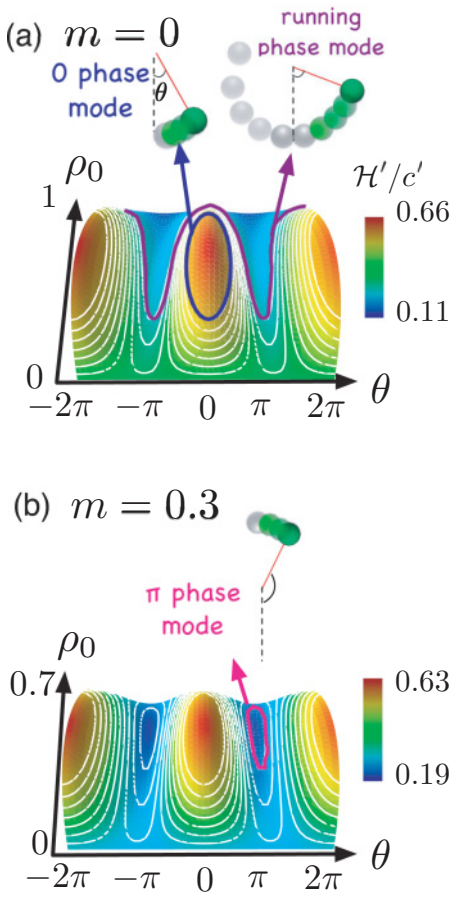

FIG. 3. (Color online) Contour lines of Eq. (24) for (a) $m = 0$ and (b) 0.3 with $\delta_{dd} = 0.3c'(>0)$, represented as white. The bold lines show the phase modes written in the figures, respectively.

C. Josephson effect for two pendulums

Here we discuss the dynamics in Eqs. (9) to (12). Solving the equations numerically using the fourth-order Runge–Kutta method, we obtain several characteristic results for two interacting nonrigid pendulums. In the calculations, we estimate that the interaction parameters satisfy the relations $c'/c_{dd}^- = 11$ and $c''/c_{dd}^- = 12$, which are determined from the order estimations $c_{dd}^+ \sim c_{dd}^- \sim c_{dd}^z$ and $c \sim 10c_{dd}^+$. The orders between the spin-exchange interactions and MDDIs have been discussed by Yi and Pu [22]. In this subsection, we denote the pendulums having angles θ and θ_m as θ and θ_m pendulums, respectively, considering the dynamics from the time developments of the canonically conjugate variables (in Sec. III C1) and the Hamiltonian (in Sec. III C2).

1. Modes in the dynamics of four variables

First, we present the typical 0–π phase mode for which θ and θ_m oscillate around $\theta = 0$ and $\theta_m = \pi$, respectively, as shown in Figs. 4(a) and 4(b). The phase mode is clearly obtained by applying small deviations from the stationary solution, Eq. (18). Considering the motion of the pendulums, the θ and θ_m pendulums make small oscillations around 0 and π as the lengths grow and shrink. The features of the oscillations

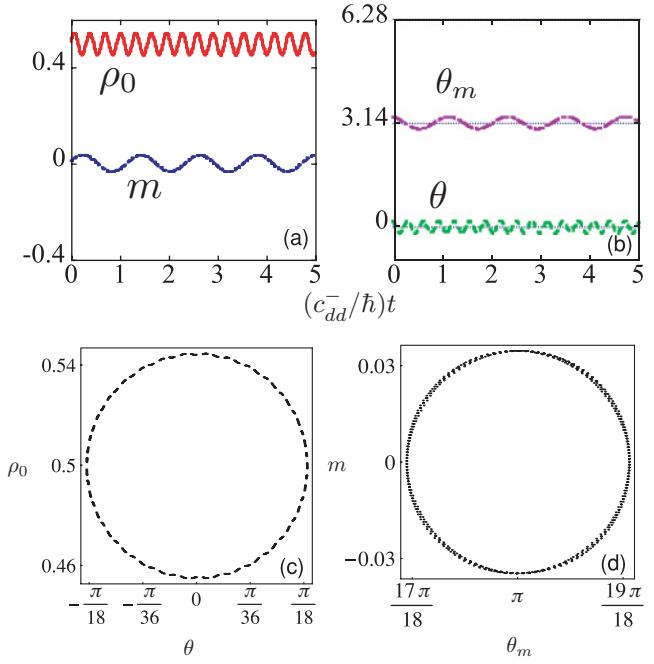

FIG. 4. (Color online) Typical 0–π phase mode. The dynamics of the four variables ρ_0, m, θ, and θ_m in (a) and (b) and the phase projections of the motions in $\{\rho_0, \theta\}$ and $\{m, \theta_m\}$ in (c) and (d) are given for $\rho_0(0) = 0.51$, $m(0) = 0.01$, $\theta(0) = \pi/18$, and $\theta_m(0) = 19\pi/18$.

are represented by trajectories projected in the phase spaces $\{\rho_0, \theta\}$ Figs. 4(c) and $\{m, \theta_m\}$ 4(d). Since the trajectory is confined to a simple closed orbit, we can see that the motion of the pendulums is similar to that of two independent pendulums, namely a periodic motion. On the other hand, changing $m(0) = 0.01$ to $m(0) = 0.36$, we obtain the quasi-0–π phase mode, shown in Fig. 5. The trajectory plotted in Fig. 5(c) is not an orbit, and hence, we regard the spread trajectory as evidence of chaotic motion of the θ pendulum. In order to investigate the chaotic motions, we plot Poincaré mappings in Fig. 6. The mappings represent projections of the cross sections at $t = nT$ ($n = 1, 2, \ldots$), where the period T is given by eigenfrequencies in the systems, providing direct evidence of chaotic motion for the 0–π phase modes, because there is only one point in the Poincaré mappings where the motions are not chaotic but periodic. However, it is unexpected that the typical 0–π phase mode should be chaotic. Therefore, we conclude that the motions of the two pendulums are essentially chaotic, and thus, the dynamics do not occur on a contour line of the 0 phase mode. The θ_m pendulum is also not a dynamic on a contour line of the π phase mode.

Setting $m(0) = 0.37$, where the other initial conditions are same as the 0–π phase mode, we can produce the 0–*running* phase mode in Fig. 7. The phase mode shows that the θ pendulum oscillates around $\theta = 0$ with a small amplitude chaotically, whereas the θ_m pendulum rotates continuously, given by the dynamics of θ_m in Fig. 7(b). The θ_m pendulum has a long stay around $\theta_m = 2n\pi$, which can be understood by Fig. 7(b).

Thus, we can obtain the transition from the 0–π phase mode to the 0–*running* phase mode by changing $m(0)$.

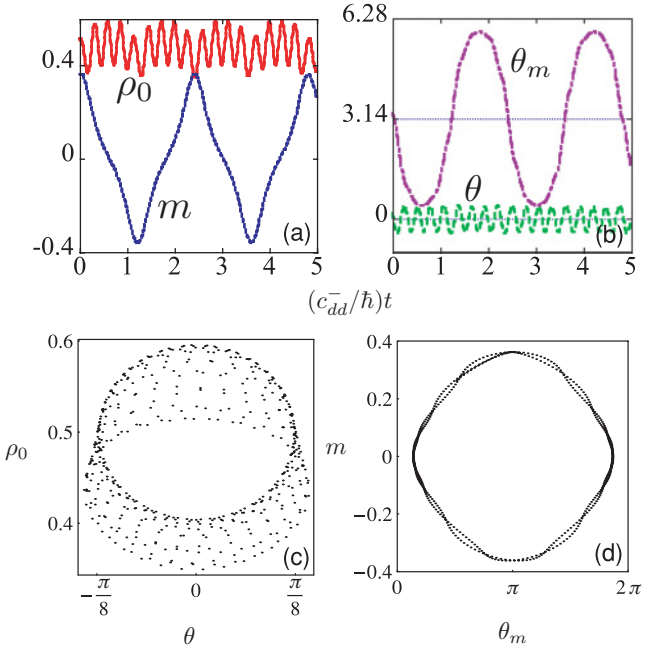

FIG. 5. (Color online) Quasi-0–π phase mode for $\rho_0(0) = 0.51$, $m(0) = 0.36$, $\theta(0) = \pi/18$, and $\theta_m(0) = 19\pi/18$.

Third, the *running–running* phase mode is shown in Fig. 8. The solutions show that the motions of the pendulums are rotations with different angular frequencies.

Fourth, we present the $2n\pi$ & *running*–2π phase mode in Fig. 9, where n is an integer. In this mode, the dynamics of the two pendulums show strange and interesting motions. Especially, the θ pendulum repeats an oscillation around $\theta = 2n\pi$ and a rotation from $\theta = 2n\pi$ to $(2n + 1)\pi$. The dynamics indicates a transition from the contour lines of the 2π phase

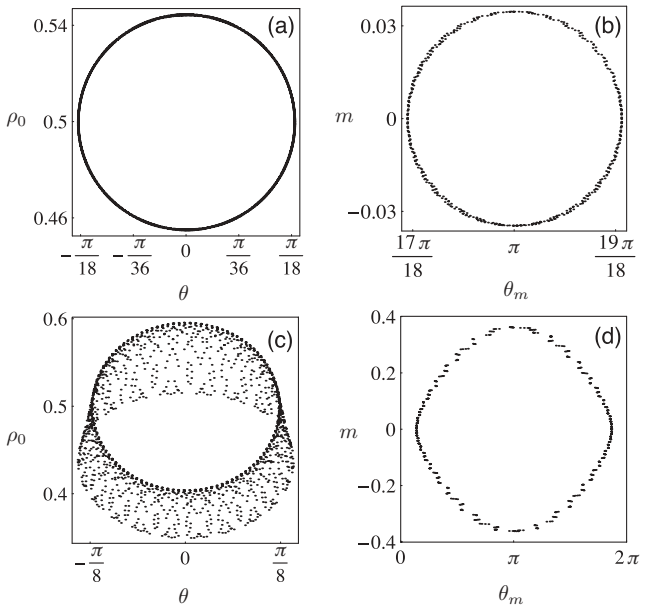

FIG. 6. Poincaré mappings for the 0–π modes within $(c_{dd}^-/\hbar)t = 500$. The upper and lower figures show the projections of the Poincaré sections at $T = 2\pi/\omega_{\rho_0-}$ for the phase spaces $\{\rho_0, \theta\}$ and $2\pi/\omega_{m-}$ for $\{m, \theta_m\}$ in Figs. 4 and 5, respectively.

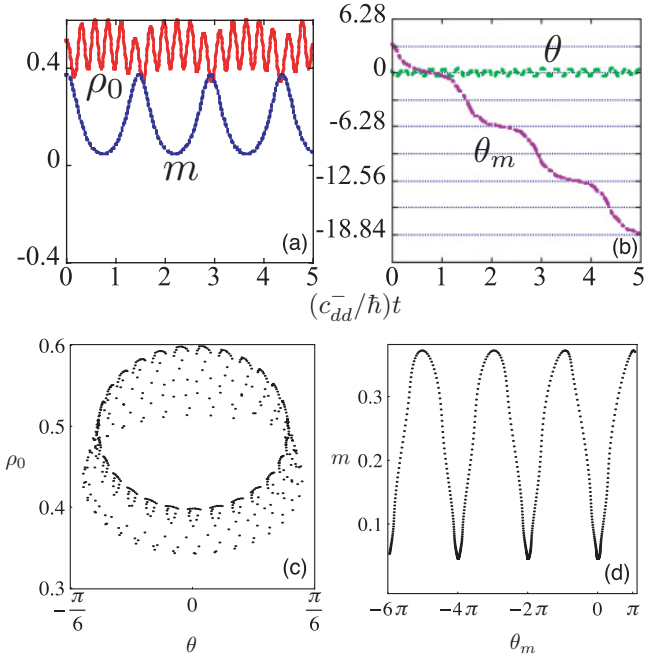

FIG. 7. (Color online) 0–*running* phase mode for $\rho_0(0) = 0.51$, $m(0) = 0.37$, $\theta(0) = \pi/18$, and $\theta_m(0) = 19\pi/18$.

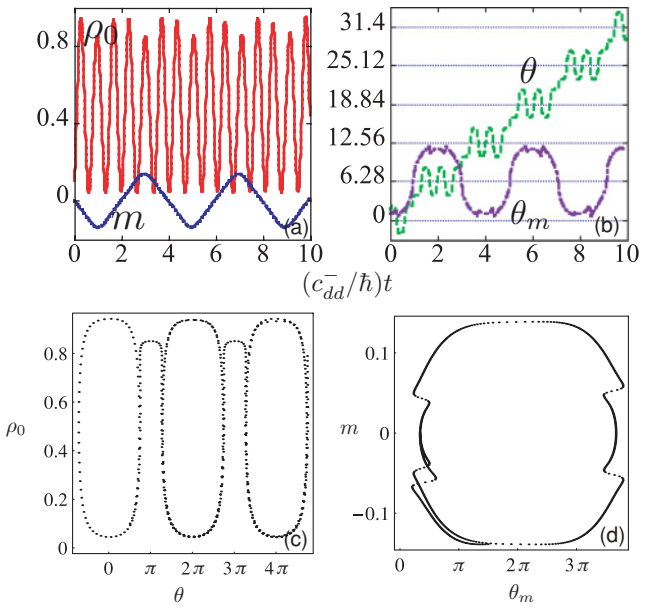

FIG. 9. (Color online) $2n\pi$ & *running*–2π phase mode for $\rho_0(0) = 0.1$, $m(0) = 0$, and $\theta(0) = \pi/2$, $\theta_m(0) = \pi/3$.

mode to another line of the *running* phase mode, which is shown clearly in Fig. 9(c). Due to this transition, transitions should occur for $\dot{\mathcal{H}} = 0$ in $\{m, \theta_m\}$. Also, the θ_m pendulum has a time average of $\langle\theta\rangle = 2\pi$. However, the pendulum repeats a rotation from $\theta \simeq 0$ to 4π and returns to $\theta \simeq 0$.

We obtain the motions of a single nonrigid pendulum in Fig. 10 and two rigid pendulums in Fig. 11, namely the *single nonrigid pendulum* and *two rigid pendulums* phase modes. For the single pendulum, the θ pendulum oscillates around $\theta = 0$, whereas the length of the θ_m pendulum grows and shrinks without an oscillation because $\theta_m = 0$. The phase space in Fig. 10(c) shows a single trajectory, indicating dynamics like that of a rigid pendulum. On the other hand, Figs. 11(a) and 11(b) show the *running–running* mode for rigid pendulums given by the constants ρ_0 and m. Then, Figs. 11(c) and 4(d) are very difficult solutions for understanding the dynamics. The θ pendulum exponentially deviates from the initial angle to $\theta = \pi$. The θ_m pendulum, however, exhibits the rotation of a rigid pendulum.

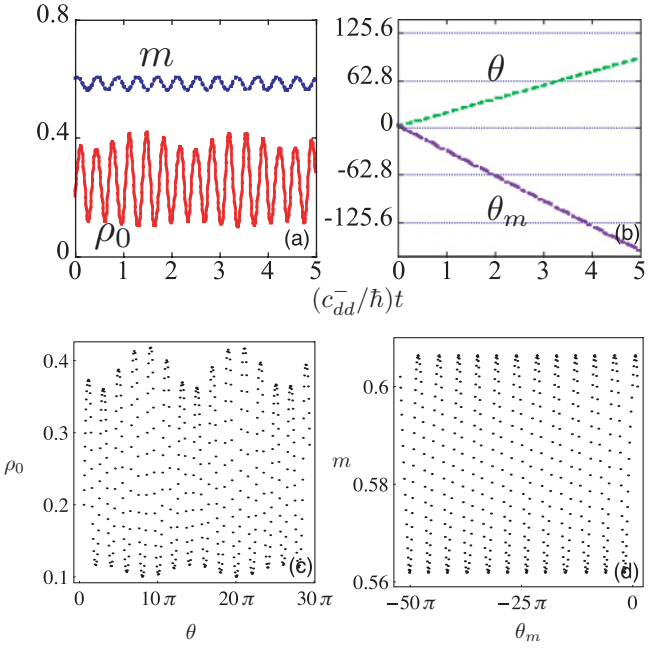

FIG. 8. (Color online) *running–running* phase mode for $\rho_0(0) = 0.6$, $m(0) = 0.2$, $\theta(0) = \pi/2$, and $\theta_m(0) = \pi$.

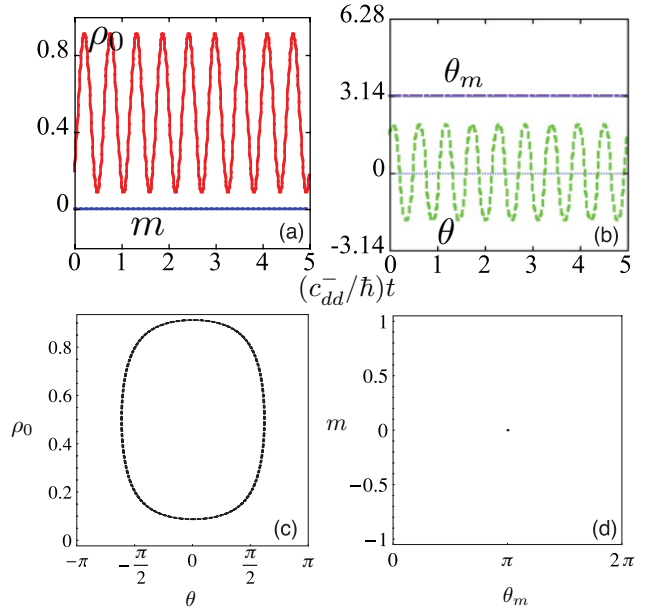

FIG. 10. (Color online) *single nonrigid pendulum* phase mode for $\rho_0(0) = 0.2$, $m(0) = 0$, $\theta(0) = \pi/2$, and $\theta_m(0) = \pi$.

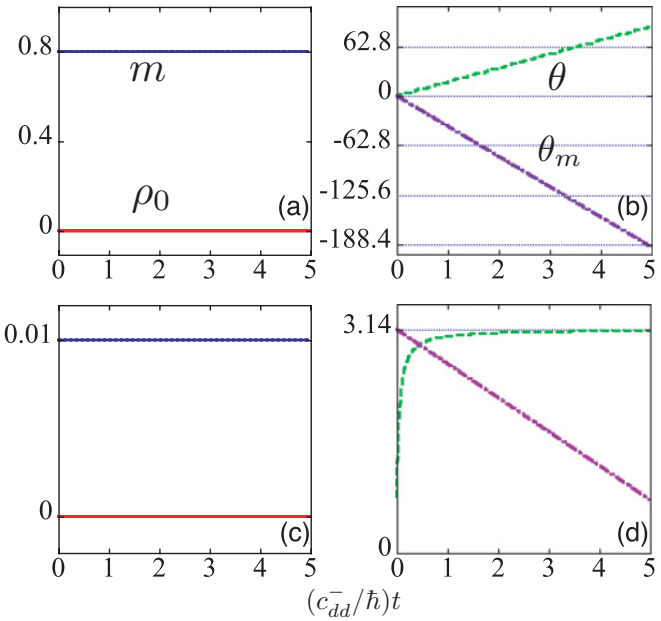

FIG. 11. (Color online) The motion of two rigid pendulums for the initial conditions $\rho_0(0) = 0, m(0) = 0.8, \theta(0) = 0$, and $\theta_m(0) = 0$ for (a) and (b), and $\rho_0 = 0, m = 0.01, \theta = \pi/4$, and $\theta_m = \pi$ for (c) and (d).

2. *Contour lines of the Hamiltonian*

Here we discuss the various modes for two pendulums from the Hamiltonians.

It is impossible to plot the contour lines for the total Hamiltonian, namely Eq. (13), because of the four dimensions given by ρ_0, m, θ, and θ_m. By considering the Hamiltonian of the θ pendulum $\mathcal{H}_\theta$ and the θ_m pendulum $\mathcal{H}_{\theta_m}$, however, the features of the motions of the pendulums can be obtained.

As mentioned in Sec. II B, $\mathcal{H}$ is a conserved value. However, $\mathcal{H}_\theta$, $\mathcal{H}_{\theta_m}$, and $\mathcal{H}_{int}$ are not conserved. Figure 12 shows the time development of these Hamiltonians, indicating the nonconservation, noting though that the values in (a) exhibit only small oscillations that do suggest energy conservation. Therefore, the trajectory in the phase spaces does not have to follow a contour line. As examples, we show the trajectories and contour lines for the 0–π and $2n\pi$ & *running*–2π phase modes in Fig. 13. Naturally, the contour lines change with time because $\mathcal{H}_\theta$ and $\mathcal{H}_{\theta_m}$ include the parameters $m(t)$ and $\rho_0(t)$, which are time dependent. In Fig. 13, we plot the lines for the time averages $m = \langle m \rangle$ and $\rho_0 = \langle \rho_0 \rangle$ in $\mathcal{H}_\theta$ and $\mathcal{H}_{\theta_m}$. The trajectories of the 0–π phase mode almost follow the contour lines in Figs. 13(a)

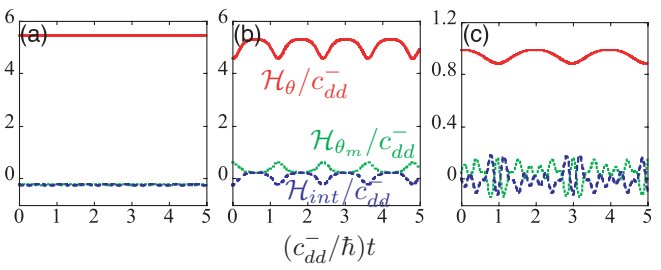

FIG. 12. (Color online) Time development of the Hamiltonians. (a), (b), and (c) have the same initial conditions as for Figs. 4, 5, and 9, respectively.

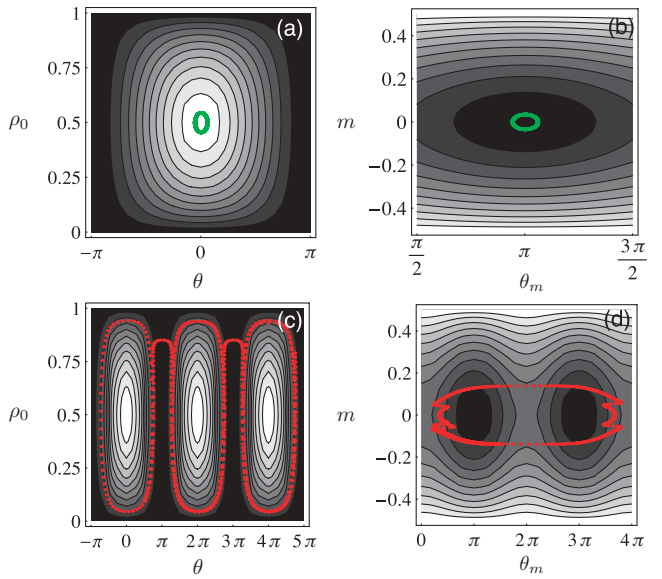

FIG. 13. (Color online) Trajectories and contour lines for the 0–π, (a) and (b), and $2n\pi$ & *running*–2π phase modes, (c) and (d). The trajectories are shown as green (right gray) lines in the 0–π mode and red (dark gray) dots in the $2n\pi$ & *running*–2π mode. The lines are given by Eq. (14) for $m = \langle m \rangle \simeq 0$ in (a) and (c) and Eq. (15) for $\rho_0 = \langle \rho_0 \rangle \simeq 0.5$ in (b) and 0.47 in (d). The magnitude of the Hamiltonians increases from black to white.

and 13(b). On the other hand, for the $2n\pi$ & *running*–2π phase mode of (c) and (d), the trajectories do not follow the lines. However, the transition from the 0 to *running* phase modes is clearly seen in $\{\rho_0, \theta\}$. An important result is that the dynamics of the θ_m pendulum cannot be discussed as transitions between the 0, π and *running* phase modes.

IV. CONCLUSION

By introducing the single-mode approximation into the spin-1 GP equations with the magnetic dipole–dipole interactions, we show the transitions between the three states, which are analogous with Josephson junctions of a ring of three superconductors. Furthermore, deriving the canonical equations of motion from the Josephson equations, the Josephson junctions are found to also be analogous with two nonrigid pendulums having interactions with each other. First, in order to consider a simple nonrigid pendulum, we assume that the shapes of the condensates are spheres. In this way, we review well-known three-phase nodes, the 0, π and *running* phase modes. Second, we numerically solve the equations for two nonrigid pendulums, showing several motions: the 0–π, 0–*running*, *running*–*running*, $2n\pi$ & *running*–2π, *single pendulum*, and *two rigid pendulum* phase modes. Finally, we discuss the transition between the modes from the nonconserved Hamiltonians $\mathcal{H}_\theta$, $\mathcal{H}_{\theta_m}$, and $\mathcal{H}_{\rm int}$.

We consider that the Josephson effect, which has been found in various phenomena from condensed matter physics to classical physics, is a universal and important physical phenomenon. In this study, the effect was discussed only in relation to BECs. However, we expect that the study of the Josephson effect of the three states will be useful in many other fields beyond atomic BECs.

ACKNOWLEDGMENTS

M. Y. acknowledges the support of a Research Fellowship of the Japan Society for the Promotion of Science for Young Scientists (Grant No. 209928). M. T. acknowledges the support of a Grant-in Aid for Scientific Research from JSPS (Grant No. 21340104) and a Grant-in-Aid for Scientific Research on Priority Areas from MEXT (Grant No. 17071008).

[1] B. D. Josephson, Phys. Lett. **1**, 251 (1962).
[2] P. W. Anderson and J. M. Rowell, Phys. Rev. Lett. **10**, 230 (1963).
[3] R. P. Feynman, R. B. Leighton, and M. Sands, *The Feynman Lectures on Physics*, Vol. III (Addison-Welsey, New York, 1965), Chap. 21, p. 21-14.
[4] K. Maki and T. Tsuneto, Prog. Theor. Phys. **52**, 773 (1974).
[5] R. A. Webb, R. L. Kleinberg, and J. G. Wheatley, Phys. Lett. **A48**, 421 (1974).
[6] A. Smerzi, S. Fantoni, S. Giovanazzi, and S. R. Shenoy, Phys. Rev. Lett. **79**, 4950 (1997)
[7] S. Raghavan, A. Smerzi, S. Fantoni, and S. R. Shenoy, Phys. Rev. A **59**, 620 (1999).
[8] M. Albiez, R. Gati, J. Fölling, S. Hunsmann, M. Cristiani, and M. K. Oberthaler, Phys. Rev. Lett. **95**, 010402 (2005).
[9] W. Zhang, D. L. Zhou, M.-S. Chang, M. S. Chapman, and L. You, Phys. Rev. A **72**, 013602 (2005).
[10] M.-S. Chang, Q. Qin, W. Zhang, L. You, and M. S. Chapman, Nature Phys. **1**, 111 (2005).
[11] S. Yi, L. You, and H. Pu, Phys. Rev. Lett. **93**, 040403 (2004).
[12] Y. Kawaguchi, H. Saito, and M. Ueda, Phys. Rev. Lett. **97**, 130404 (2006).
[13] H. Mäkelä and K.-A. Suominen, Phys. Rev. A **75**, 033610 (2007).
[14] Y. Kawaguchi, H. Saito, and M. Ueda, Phys. Rev. Lett. **96**, 080405 (2006).
[15] A. Griesmaier, J. Werner, S. Hensler, J. Stuhler, and T. Pfau, Phys. Rev. Lett. **94**, 160401 (2005).
[16] J. Stuhler, A. Griesmaier, T. Koch, M. Fattori, T. Pfau, S. Giovanazzi, P. Pedri, and L. Santos, Phys. Rev. Lett. **95**, 150406 (2005).
[17] T. Lahaye, T. Koch, B. Fröhlich, M. Fattori, J. Metz, A. Griesmaier, S. Giovanazzi, and T. Pfau, Nature **448**, 672 (2007).
[18] R. Cheng, J.-Q. Liang, and Y. Zhang, J. Phys. B: At. Mol. Opt. Phys. **38**, 2569 (2005).
[19] S. Yi and H. Pu, Phys. Rev. Lett. **97**, 020401 (2006).
[20] Here we can only mention $c_{dd}^{x} = c_{dd}^{y} = c_{dd}^{z}$, namely $c_{dd}^{-} = 0$, in the spherical geometry and non uniform density. The dipolar effect disappear in the geometry and density given by Gaussian form [11]. However, we do not assume the Gaussian density, not discussing the Josephson oscillation under $c_{dd}^{x,y,z} = 0$.
[21] J. Stenger, S. Inouye, D. M. Stamper-Kurn, H.-J. Miesner, A. P. Chikkatur, and W. Ketterle, Nature **396**, 345 (1998).
[22] S. Yi and H. Pu, in *Electromagnetic, Magnetostatic and Exchange Interaction Vortices in Confined Magnetic Structures*, edited by E. O. Kamenetskii (Research Signpost, Kerala, 2009).